N Aiba et al.

Diamagnetic equation for plasmas with fast flow and its application to ELM analysis in JT-60U and JET-ILW

Diamagnetic MHD equations for plasmas with fast flow and its application to ELM analysis in JT-60U and JET-ILW

N. Aiba[1], C. Giroud[2], M. Honda[3], E. Delabie[4], S. Saarelma[2], L. Frassinetti[5], I. Lupelli[2], S. Pamela[2], H. Urano[3], C. Maggi[2] and JET Contributors[*6]

[1]National Institutes for Quantum and Radiological Science and Technology, Rokkasho, Aomori 039-3212, Japan
[2]Culham Centre for Fusion Energy, Culham Science Centre, Abingdon OX14 3DB, UK
[3]National Institutes for Quantum and Radiological Science and Technology, Naka, Ibaraki 319-1112 Japan
[4]Oak Ridge National Laboratory, Oak Ridge TN 37831, USA
[5]Division of Fusion Plasma Physics, KTH, SE-10041 Stockholm, Sweden
[6]EUROfusion Consortium, JET, Culham Science Centre, Abingdon, OX14 3DB, UK

Corresponding Author: aiba.nobuyuki@qst.go.jp

Abstract:

Diamagnetic MHD equations and the corresponding Frieman-Rotenberg (F-R) equation were derived to analyze MHD stability with the ion diamagnetic drift effect in rotating tokamak plasmas. The MINERVA-DI code was developed to solve the F-R equation to analyze the edge localized mode (ELM) stability in JT-60U and JET-ILW. It is found that rotation in both toroidal and poloidal directions can destabilize ELMs, and this destabilizing effect can minimize the stabilization effect due to the ion diamagnetic drift. These rotation effects are indispensable for discussing the pedestal stability when the toroidal mode number of the ELM is high as predicted in JT-60U and JET-ILW.

1 Introduction

In H-mode regime in tokamak plasmas, a large ELM, called type-I ELM, sometimes induces large heat load to divertor periodically. Since the heat load is unacceptable for ITER and DEMO reactors, it is necessary to predict precisely the threshold pedestal pressure triggering the ELM. The threshold pressure has been predicted with ideal MHD stability analysis, but recently, the type-I ELM in JET with ITER like wall (JET-ILW) can appear even when the pedestal pressure gradient is about half of the numerical prediction[1, 2]. The toroidal mode number n of the ELM in JET-ILW is higher than that in JET with

---

carbon wall (JET-C), though such high-n MHD modes can be stabilized by the ion diamagnetic drift (ω_{*i}) effect[3]. On the other hand, it was identified that plasma rotation in toroidal and poloidal directions can destabilize such high-n ELMs, and improves the reliability of numerical analysis of ELM stability in JT-60U[4].

In this study, we revisit the ELM stability of the plasmas by paying attention to not only deuterium rotation but also the ω_{*i} effects. To realize this objective, we have developed a new MHD model, named a diamagnetic MHD model, and the corresponding extended Frieman-Rotenberg (F-R) equation, which can be solved numerically with the MINERVA-DI code[5]; the details are written in Sec. 2. With this code, we analyze the rotation and ω_{*i} effects on type-I ELM stability in JT-60U and JET-ILW in Sec. 3. Section 4 presents a summary and discussion of this study.

2 Diamagnetic MHD equations and extended Frieman-Rotenberg equation

To investigate the ω_{*i} effect on MHD stability in rotating plasmas, we revisit the basic equations based on the ordered fluid equations[6]. A well-known ideal MHD model can be obtained by assuming that $\lambda = V_0/V_{thi} \sim O(1)$ and $\nu = \omega_0/\Omega_i = O(\delta)$, where Ω_i is the ion cyclotron frequency, V_{thi} is the ion thermal velocity, $\delta = \rho_i/L$, ρ_i is the ion Larmor radius, and Ω_0, V_0, L are the characteristic values of frequency, velocity and length, respectively. This model can identify ideal MHD stability in both static and rotating plasmas, but cannot discuss the ω_{*i} effect. Another well-know "drift model" can be derived by assuming $\lambda \sim O(\delta)$ and $\nu \sim O(\delta^2)$ and realizes to take into account finite Larmor radius effects, including the ω_{*i} effect, in the stability analysis[7]. However, since $\lambda \sim O(\delta)$ means that the $\boldsymbol{E} \times \boldsymbol{B}$ drift velocity is much smaller than V_{thi}, the plasma rotation velocity should be kept much smaller than V_{thi}.

To overcome these restrictions, we introduce the ordering parameter by $\lambda = \delta^\alpha$ with $0 < \alpha \leq 0.5$. After some manipulations with this parameter, the diamagnetic MHD equations can be derived from the ordered fluid equations as[5]

$$\frac{\partial N}{\partial t} + \nabla \cdot (N\boldsymbol{V}_{MHD}) = 0, \tag{1}$$

$$m_i N \left[\frac{\partial \boldsymbol{V}_{MHD}}{\partial t} + (\boldsymbol{V}_{MHD} \cdot \nabla)\boldsymbol{V}_{MHD} + (\boldsymbol{V}_{*i} \cdot \nabla)\boldsymbol{V}_E \right] = \boldsymbol{J} \times \boldsymbol{B} - \nabla P, \tag{2}$$

$$\frac{\partial P}{\partial t} + (\boldsymbol{V}_{MHD} \cdot \nabla)P + \Gamma P \nabla \cdot \boldsymbol{V}_{MHD} = 0, \tag{3}$$

$$\frac{\partial \boldsymbol{B}}{\partial t} = \nabla \times \boldsymbol{E}, \tag{4}$$

$$\boldsymbol{E} + \boldsymbol{V}_{MHD} \times \boldsymbol{B} = 0, \tag{5}$$

$$\nabla \times \boldsymbol{B} = \mu_0 \boldsymbol{J}. \tag{6}$$

Here N is the ion number density, m_i is the ion mass, $\boldsymbol{J}$ is the plasma current, $\boldsymbol{B}$ is the magnetic field, P is the plasma pressure, Γ is the ratio of specific heat, $\boldsymbol{E}$ is the electric

field and μ_0 is the permeability in the vacuum. The definitions of velocity vectors are

$$\boldsymbol{V}_{MHD} = \boldsymbol{V}_E + V_\parallel \frac{\boldsymbol{B}}{|\boldsymbol{B}|}, \tag{7}$$

$$\boldsymbol{V}_E = \frac{\boldsymbol{E} \times \boldsymbol{B}}{|\boldsymbol{B}|^2}, \tag{8}$$

$$\boldsymbol{V}_{*i} = \frac{1}{eZ_{eff}N|\boldsymbol{B}|^2}\boldsymbol{B} \times \nabla p_i, \tag{9}$$

where $V_\parallel$ is the velocity parallel to $\boldsymbol{B}$, $\boldsymbol{V}_E$ is the $E \times B$ drift velocity, $\boldsymbol{V}_{*i}$ is the ion diamagnetic drift velocity, e is the quantum of electricity, Z_{eff} is the effective charge, and p_i is the ion pressure. By introducing the Lagrangian displacement vector $\boldsymbol{\xi}$ and assuming the incompressible condition $\nabla \cdot \boldsymbol{\xi} = 0$, we can derive the extended Frieman-Rotenberg equation, which is the linearized equation of motion of Eqs. (1)-(6), as

$$\rho_0 \frac{\partial^2 \boldsymbol{\xi}}{\partial t^2} + 2\rho_0(\boldsymbol{V}_{0,MHD} \cdot \nabla)\frac{\partial \boldsymbol{\xi}}{\partial t} + \rho_0(\boldsymbol{V}_{0,*i} \cdot \nabla)\frac{\partial \boldsymbol{\xi}_\perp}{\partial t} = \boldsymbol{F}_{MHD} + \boldsymbol{F}_{*i}, \tag{10}$$

$$\boldsymbol{F}_{MHD} = (\nabla \times \nabla \times (\boldsymbol{\xi} \times \boldsymbol{B}_0)) \times \boldsymbol{B}_0 + \boldsymbol{J}_0 \times \nabla \times (\boldsymbol{\xi} \times \boldsymbol{B}_0)$$
$$+ \nabla [\boldsymbol{\xi} \cdot \nabla P_0 + \Gamma P_0 \nabla \cdot \boldsymbol{\xi}] + \rho(\boldsymbol{V}_{0,MHD} \cdot \nabla)(\boldsymbol{V}_{0,MHD} \cdot \nabla)\boldsymbol{\xi}$$
$$+ \nabla \cdot [\rho_0\boldsymbol{\xi}(\boldsymbol{V}_{0,MHD} \cdot \nabla)\boldsymbol{V}_{0,MHD} - \rho_0\boldsymbol{V}_{0,MHD}(\boldsymbol{V}_{0,MHD} \cdot \nabla)\boldsymbol{\xi}]$$
$$+ \nabla \otimes \rho_0 [\boldsymbol{\xi} \otimes (\boldsymbol{V}_{0,MHD} \cdot \nabla)\boldsymbol{V}_{0,MHD} - \boldsymbol{V}_{0,MHD} \otimes (\boldsymbol{V}_{0,MHD} \cdot \nabla)\boldsymbol{\xi}], \tag{11}$$

$$\boldsymbol{F}_{*i} = \nabla \otimes [\rho_0\boldsymbol{\xi} \otimes (\boldsymbol{V}_{0,*i} \cdot \nabla)\boldsymbol{V}_{0,MHD} - \rho_0\boldsymbol{V}_{0,*i} \otimes (\boldsymbol{V}_{0,MHD} \cdot \nabla)\boldsymbol{\xi}]$$
$$+ \frac{\rho_0}{eZ_{eff}N_0B_0^2}[\{(\nabla \cdot (\boldsymbol{\xi} \times \nabla P_0))\boldsymbol{B}_0 - (\boldsymbol{B}_0 \cdot \nabla P_0)\nabla \times \boldsymbol{\xi}\} \cdot \nabla]\boldsymbol{V}_{0,E}. \tag{12}$$

Here $\rho_0 = m_i N_0$ is the mass density, and the subscript 0 expresses the equilibrium quantity. Note that the flute approximation $(\boldsymbol{B}_0 \cdot \nabla)\boldsymbol{\xi} << 1$ is applied for deriving Eq.(10).

In this study, we assume the isothermal condition on each magnetic surface $T_0 = T_i(\psi) + T_e(\psi) = T_0(\psi)$ due to strong parallel heat conductivity[8], and hence, the profiles of equilibrium pressure and density should depend on not only the radial but also poloidal directions[5]. Here, T_i (T_e) is the ion (electron) temperature, and ψ is the poloidal magnetic flux normalized as 0 (1) on axis (surface).

3 Impact of rotation and ion diamagnetic drift effects on ELM stability in JT-60U and JET-ILW

In this section, we analyze the stability to a peeling-ballooning mode in JT-60U and JET-ILW type-I ELMy H-mode plasmas. To take into account both the rotation and the ω_{*i} effects on the stability, Eq.(10) is solved with the MINERVA-DI code[5].

3.1 Results in JT-60U

The shot number of the JT-60U plasma is E49229 whose ELM frequency is $\sim 45[\text{Hz}]$. In this discharge, the toroidal magnetic field on axis and the plasma current are $B_{t0} = 4.0[\text{T}]$
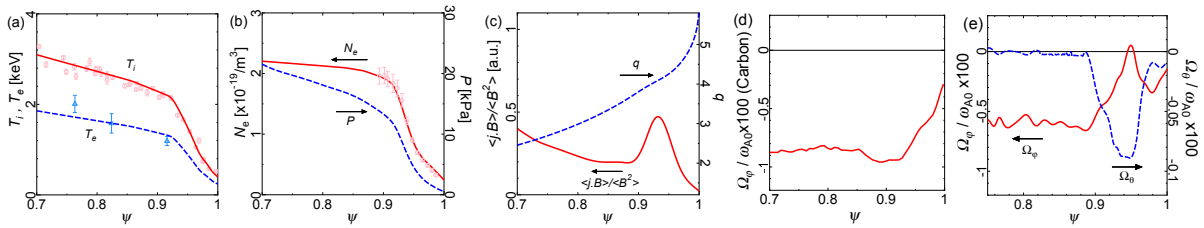
FIG. 1:   *Profiles of the JT-60U E49229 plasma; (a) T_i and T_e, (b) N_e and P, (c) $\langle \boldsymbol{j} \cdot \boldsymbol{B} \rangle / \langle B^2 \rangle$ and q, (d) Ω_ϕ of impurity (carbon), and (e) Ω_ϕ and Ω_θ of bulk plasma (deuterium), respectively.*

and $I_p = 1.6$[MA], and the plasma rotates in the direction counter to the plasma current due to the external momentum input by neutral beam injection (NBI). The profiles of T_i and rotation velocity of impurity (carbon) were measured with modulation charge exchange recombination spectroscopy (MCXRS), those of T_e and N_e were measured with Thomson scattering (TS), and in addition, the N_e profile near edge pedestal was measured with lithium beam probe (LiBP)[9]. Unfortunately, the spatial resolution of TS is not enough, and hence, the T_e profile used in this study is determined to be $T_e = 0.6T_i$; this coefficient is determined to follow the TS measurement data at $\psi \geq 0.8$. The impurity rotation profile is determined by overlaying the MCXRS data just before ELM crashes[10]. The ion density is determined by $N = N_e(Z - Z_{eff}/(Z - 1))$, which is derived from the definition of Z_{eff} and charge neutrality condition with the assumption that an impurity contains only one type of atom, where Z is the charge of the impurity. The main impurity in JT-60U is carbon with $Z = 6$, and $Z_{eff} = 2.8$ in the E49229 plasma. The current density near pedestal is determined based on the neoclassical theory with the ACCOME code[11]. The profiles of T_i, T_e, N_e, P, $\langle \boldsymbol{j} \cdot \boldsymbol{B} \rangle / \langle B^2 \rangle$, q and toroidal rotation frequency, Ω_ϕ, of impurity are shown in Fig. 1 (a)-(d).

The rotation profile of bulk plasma (deuterium) is estimated based on the neoclassical theory with measured impurity toroidal rotation by the CHARROT code. The CHARROT code has been developed to estimate rotation and the radial electric field by extracting the modules from an integrated simulation code TOPICS[12]. It has already been confirmed that the neoclassical transport solver implemented in CHARROT successfully reproduces profiles of poloidal rotation and the radial electric field in the edge region of the JT-60U L- and H-mode discharges[13]. Figure 1 (e) shows the profiles of deuterium rotation frequency in the toroidal and poloidal directions, Ω_ϕ and Ω_θ; these are estimated by CHARROT. It should be noted that MINERVA-DI is coded in right-handed system and ω_{*i} is negative near pedestal in JT-60U (and JET-ILW) whose toroidal magnetic field and plasma current are clockwise from the top.

The ELM stability diagram is identified by analyzing the stability of the equilibria which have different pedestal pressure gradient and edge current density. These are changed by adjusting the height of pressure pedestal and the amount of bootstrap current near the pedestal; the details are written in [14]. We scan a range of toroidal mode number $1 \leq n \leq 60$ of MHD modes with the boundary condition that JT-60U vacuum
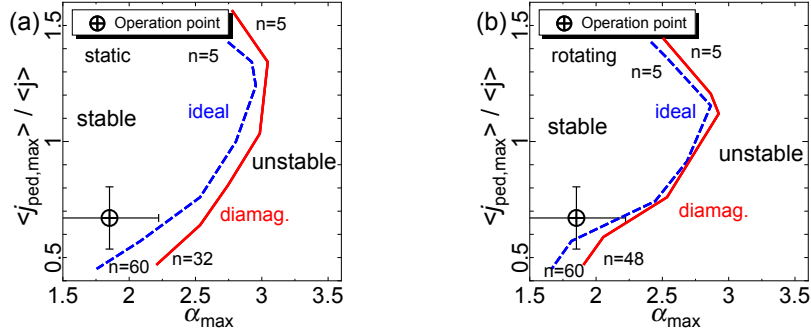
FIG. 2: *Stability diagrams of the JT-60U E49229 plasma in (a) the static and (b) rotating cases on the $(\langle j_{ped,max}\rangle/\langle j\rangle, \alpha_{max})$ plane; the width of error bars on the operation point (O.P.) are determined to be $\pm 20\%$ in α and $\langle j\rangle$. In the static case, the O.P. exists in the stable region, and the ω_{*i} effect pushes the stability boundary away from the O.P.. In the rotating case, the diamagnetic stability boundary becomes close to the ideal one, and the both stability boundaries are within the error bars; $\Delta\alpha_{max}$ determined with the diamagnetic MHD model is reduced from 40% in the static case to 20%.*

vessel acts as ideal conducting wall.

Figure 2 shows the ELM stability diagrams in (a) the static and (b) rotating cases on the $(\langle j_{ped,max}\rangle, \alpha_{max})$ plane. Here j_{ped} is the current density in pedestal region, $\langle x\rangle$ is the flux averaged value of x, $\alpha \equiv -(\mu_0/2\pi^2)(dP_{a0}/d\psi)(dV/d\psi)(V/2\pi^2 R_0)^{0.5}$ is the normalized pressure gradient, P_{a0} is the axisymmetric part of the equilibrium pressure, V is the volume, R_0 is the major radius on axis, and the subscript max expresses the maximum value in pedestal region. The numbers shown in the diagrams are the n number of the most unstable mode on the boundary near them. In the static case, the α_{max} value on the stability boundary determined with the ideal MHD model (ideal stability boundary) is about 25% larger than that on the operation point (O.P.); hereafter, we measure the difference in α_{max} between the O.P. and the stability boundary, $\Delta\alpha_{max}$, under the condition that $\langle j_{ped,max}\rangle$ is the same as that on the O.P.. The ω_{*i} effect pushes the stability boundary away from the O.P., and $\Delta\alpha_{max}$ increases to 40%. These results show that the ω_{*i} effect has large impact on the stability to the peeling-ballooning mode when plasma rotation is neglected, and this impact increases the discrepancy between the experimental and numerical results of ELM analysis.

However, by taking into account rotation effects on MHD stability, the stability boundary becomes closer to the O.P., and in particular, the ideal stability boundary is almost on the O.P.. More than anything else, the diamagnetic stability boundary becomes almost the same as the ideal one in the range $0.6 < \langle j_{ped,max}\rangle/\langle j\rangle < 1.5$. In fact, $\Delta\alpha_{max}$ determined with the diamagnetic MHD model is about 20%, which is about half of that in the static case. The results in this section evince that rotation of the bulk plasma estimated based on the neoclassical theory can have large impact on the stability to the peeling-ballooning mode. The stability boundary on the $(\langle j_{ped,max}\rangle, \alpha_{max})$ stability diagram tends to be affected by rotation in the region where $\langle j_{ped,max}\rangle$ is much smaller than that of current driven kink/peeling boundary. These results show that plasma rotation
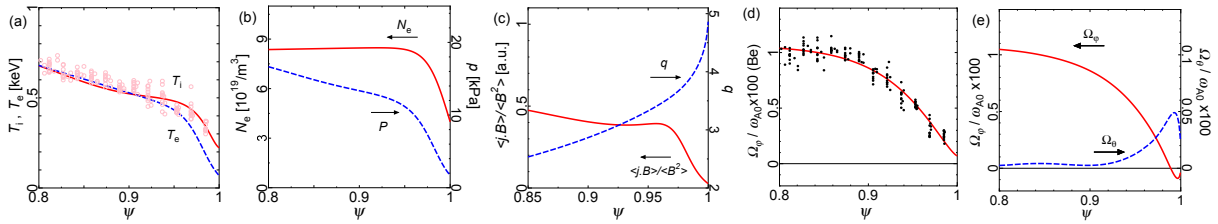
FIG. 3: Profiles of the JET-ILW 89709 plasma; (a) T_i and T_e, (b) N_e and P, (c) $\langle \boldsymbol{j} \cdot \boldsymbol{B} \rangle / \langle B^2 \rangle$ and q, (d) Ω_ϕ of impurity (carbon), and (e) Ω_ϕ and Ω_θ of bulk plasma (deuterium), respectively.

has potential to resolve the discrepancy between the experimental result and the numerical prediction of ELM stability, because the rotation destabilizes the peeling-ballooning modes and minimizes the ω_{*i} stabilizing effect on them.

3.2 Results in JET-ILW

The shot number of the JET-ILW plasma is #89709 whose ELM frequency is $\sim 40[\text{Hz}]$. In this discharge, $B_{t0} = 2.6[\text{T}]$ and $I_p = 2.5[\text{MA}]$, and the plasma rotates in the direction same as the plasma current; namely, all of them are clockwise from the top. The profiles of T_i and impurity (carbon) rotation velocity were measured with CXRS, those of T_e and N_e were measured with TS. All the profiles just before ELMs are obtained with ELM synchronization technique to improve the spatial resolution[15]. The main impurity of this plasma is beryllium with $Z = 4$, and $Z_{eff} = 1.5$. The profiles of bootstrap current and deuterium rotation are estimated by CHARROT. Note that the rotation profile of beryllium is assumed as the same as the measured one of carbon. The profiles of T_i, T_e, N_e, P, $\langle \boldsymbol{j} \cdot \boldsymbol{B} \rangle / \langle B^2 \rangle$, q, Ω_ϕ of impurity, and Ω_ϕ and Ω_θ of deuterium are shown in Fig. 3.

The ELM stability diagram is identified in the same manner introduced in the JT-60U case except the range of toroidal mode number $1 \leq n \leq 100$, and ideal conducting wall is located at $d/a = 1.3$ as the boundary condition. Figure 4 shows the ELM stability diagrams in (a) the static and (b) rotating cases on the $(\langle j_{ped,max} \rangle, \alpha_{max})$ plane. Note that since the bootstrap current in this JET-ILW plasma is small compared to that in the JT-60U plasma shown in the previous subsection, the n number of the most unstable mode becomes larger. In the static case, the α_{max} value on the stability boundary determined with the ideal MHD model (ideal stability boundary) is about 30% larger than that on the O.P., and the ω_{*i} effect widens $\Delta\alpha_{max}$ up to 45%.

However, as in the JT-60U case, deuterium rotation bring the stability boundary close to the O.P., and the ideal MHD stability boundary is within the error bars determined to be $\pm 20\%$ in α; this error bar is usually used to roughly reflect the measurement errors in the stability diagram. Though the diamagnetic MHD stability boundary is still outside the error bars, $\Delta\alpha_{max} \sim 27\%$ becomes less than two-thirds of that in the static case. These trends are qualitatively the same as those in the JT-60U case, and show that deuterium rotation plays a role on determining the ELM stability boundary in JET-ILW.
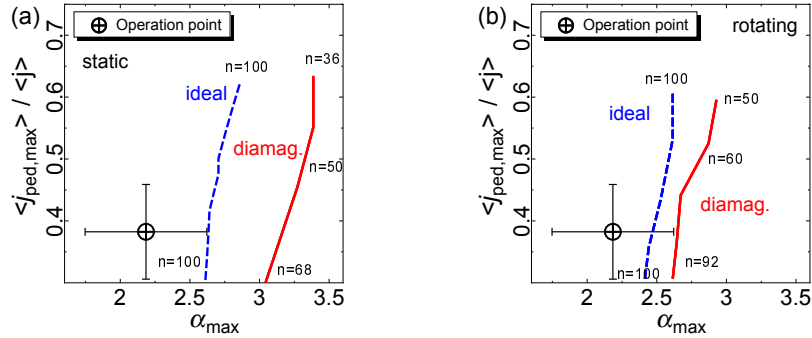
FIG. 4: Stability diagrams of the JET-ILW 89709 plasma in (a) the static and (b) rotating cases on the ($\langle j_{ped,max}\rangle/\langle j\rangle$, α_{max}) plane; the width of error bars on the operation point (O.P.) are determined to be $\pm 20\%$ in α and $\langle j\rangle$. In the static case, the O.P. exists in the stable region, and the ω_{*i} effect pushes the stability boundary away from the O.P.. In the rotating case, the ideal stability boundary is within the error bar, and the diamagnetic one shifts to the lower α_{max} side; $\Delta\alpha_{max}$ is reduced from 25% (45%) in the static case to 15% (27%) with the ideal (diamagnetic) MHD model.

4   Summary

Diamagnetic MHD equations have been derived with the ordered fluid equations in order to investigate the ion diamagnetic drift (ω_{*i}) effect on ideal MHD stability in rotating plasmas. The corresponding extended Frieman-Rotenberg (F-R) equation was obtained from these equations under the incompressible assumption, and a linear extended MHD stability code MINERVA-DI has been developed to solve this equation.

With MINERVA-DI, the stability to the peeling-ballooning mode in type-I ELMy H-mode plasmas in JT-60U and JET with ITER like wall (ILW) was analyzed. The deuterium rotation in both toroidal and poloidal directions are determined based on the neoclassical theory with the CHARROT code. When the plasma is assumed static, the ω_{*i} effect increases the threshold pressure gradient triggering the ELM due to stabilizing the peeling-ballooning mode. This trend increases the discrepancy between the experimental result and the numerical result of ELM stability analysis, because the operation point just before ELM crash exists in the stable region of the stability diagram. However, by rotating the plasma, the peeling-ballooning mode becomes more unstable, and as the result, the threshold pressure gradient determined with the ideal MHD model approaches to the operation point. In addition, the rotation can minimize the ω_{*i} stabilizing effect on the mode, and reduce the discrepancy between the experimental result and the numerical prediction of ELM stability. These physics trends have been observed in both JT-60U and JET-ILW.

In comparison with the result in JT-60U, the result of stability analysis in JET-ILW shows that the stability boundary determined with the diamagnetic MHD model is still different from that with the ideal MHD model even when plasma rotation is taken into account. The reason of this difference is still under discussion, but one possibility is the difference in temperature at pedestal. The temperatures of both deuterium and electron

in the JET-ILW plasma analyzed in this study are less than half of those in the JT-60U one, and in such a low temperature case, the impact of plasma resistivity on MHD stability will become no longer negligible. To address this issue, we will extend the physics model to include the resistivity in Ohm's law, and will investigate the importance of resistivity on the ELM stability in rotating plasmas in future.

Acknowledgment

References

[1] Giroud C et al. 2015 *Plasma Physics and Controlled Fusion* **57** 035004

[2] Maggi C F et al. 2015 *Nucl. Fusion* **55** 113031

[3] Tang W M, Connor J W and Hastie R J 1980 *Nucl. Fusion* **20** 1439

[4] Aiba N et al. 2011 *Nucl. Fusion* **51** 073012

[5] Aiba N 2016 *Plasma Phys. Control. Fusion* **58** 045020

[6] Schnack D D et al. 2006 *Phys. Plasmas* **13** 058103

[7] Hazeltine R D and Meiss J D 1992 *Plasma Confinement* (Addison-Wesley, Rwdwood City)

[8] Lao L L et al. 2005 *Fusion Sci. Tech.* **48** 968

[9] Kojima A et al. 2009 *Nucl. Fusion* **49** 115008

[10] Kamiya K et al. 2014 *Phys. Plasmas* **21** 122517

[11] Tani K, Azumi M and Devoto R S J 1992 *J. Comput. Phys.* **98** 332

[12] Honda M et al. 2013 *Nucl. Fusion* **53** 073050

[13] Honda M et al. 2015 *Nucl. Fusion* **55** 073033

[14] Aiba N, Honda M and Kamiya K 2016 *Nucl. Fusion* in press

[15] Frassinetti L et al. 2012 *Rev. Sci. Instrum.* **83** 013506